Available online at www.sciencedirect.com

ScienceDirect

journal homepage: http://www.elsevier.com/locate/acme

Original Research Article

A comparative study of transverse shrinkage stresses and residual stresses in P91 welded pipe including plasticity error

Chandan Pandey [a], *Manas Mohan Mahapatra* [b], *Pradeep Kumar* [a,*]

[a] *Department of Mechanical and Industrial Engineering, Indian Institute of Technology Roorkee, Uttrakhand 247667, India*

[b] *School of Mechanical Sciences, Indian Institute of Technology Bhubaneswar, Odisha 751013, India*

ARTICLE INFO

Article history:
Received 2 December 2017
Accepted 12 February 2018
Available online 15 March 2018

Keywords:
GTAW
Plasticity
Residual stresses
Shrinkage stresses
PWHT

ABSTRACT

The paper deals with the measurement of the residual stresses in P91 welded pipe using the blind hole drilling technique. The P91 pipe weld joints were prepared using gas tungsten arc welding process. The residual stress measurement was carried out using the strain gauge rosette that was associated with the plastic deformation of material and stress concentration effect of multi-point cutting tool. Strain gauge response was estimated experimentally using the tensile testing for the uniaxial loading while finite element analysis was performed for biaxial loading. Gas tungsten arc welds joint was prepared for conventional V-groove and narrow groove design. The corrective formulation was developed for calculating the corrected value of residual stresses from the experimentally obtained strain value. The corrected and experimental induced residual stresses values as per ASTM E837-13 were calculated for both V-groove and narrow groove design. Post weld heat treatment (PWHT) of P91 welded pipe was also conducted to study their effect on residual stresses.

1. Introduction

To overcome the CO_2 emission and lead to endeavors to improve the thermal efficiency of power plants, creep strength enhanced ferritic (CSEF) steels are selected as the candidate material for high temperature operating power plant components [1,2]. CSEF steels have been considered as superior material over austenitic stainless steel due to its attractive thermo-physical and mechanical properties [3–5]. The commonly used CSEF steels are P9, P91, and P92.

However, for long-term creep exposure the lower creep rupture life of P91 welds joint as compared to 'as-received' base metal is a serious issue [6]. The residual stresses, weld microstructure and diffusible hydrogen present in deposited metal are the main parameters which affect the weldability of

* *Corresponding author.*
E-mail addresses: chandanpy.1989@gmail.com (C. Pandey), manasfme@gmail.com (M.M. Mahapatra), kumarfme@gmail.com (P. Kumar).

https://doi.org/10.1016/j.acme.2018.02.007
1644-9665/

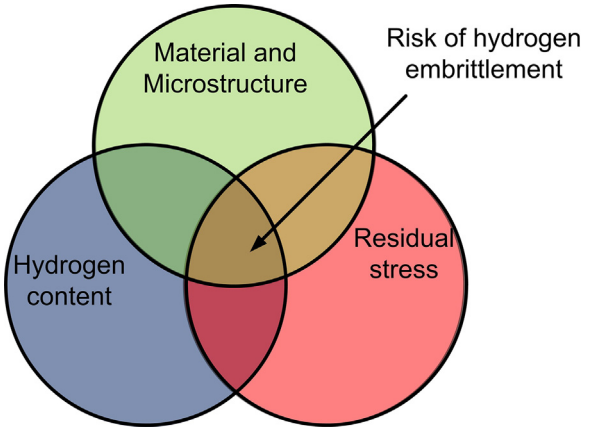

Fig. 1 – Schematic evolution of essential condition that affects weldability.

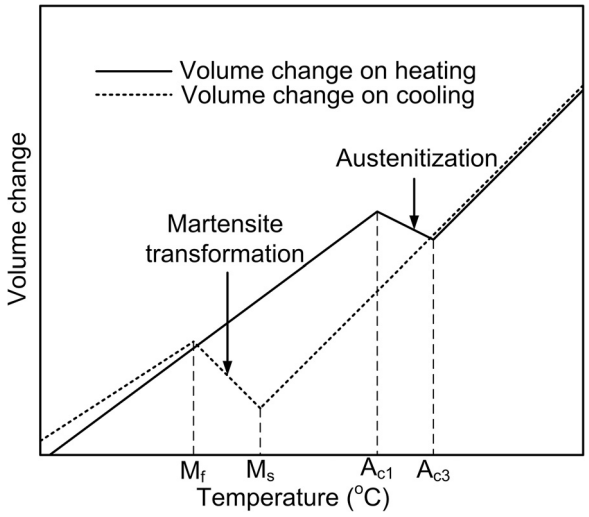

Fig. 2 – Schematic diagram of volume change during heating and cooling cycle of P91 weldments.

P91 steel. The residual stress and microstructure of P91 steel weldment can be controlled by using the proper PWHT as suggested by the researchers [2,7], but the hydrogen induced cracking (HIC) in P91 steel weld is a serious problem [8]. A combined effect of sensitive microstructure, high residual stress and sufficient level of hydrogen on HIC is shown in Fig. 1. Joining of structural component, piping and pressure vessels used in nuclear, thermal fertilizer and chemical power industries are generally carried out by the welding process that results in residual stress, shrinkage stress and distortion at remarkable level [9,10]. In welding process, the localized heating and cooling leads to the formation of complex residual stress and distortion may result in catastrophic failure of welded joint. Localized heating and cooling of base, solidification shrinkage of weld, internal constraint, external constraint like tacking, and phase transformation result in formation of residual stresses and distortion [11,12]. Compared to the weld structure, size of weld pool is very small and expansion and contraction of the weld during the weld thermal cycle is prevented by the adjacent base metal. During the heating cycle, expansion of heated zone leads to the formation of compressive residual stress and cooling cycle results in shrinkage which is prevented by the base metal. After the cooling, shrinkage resistance cause the formation of tensile residual stress in weld zone which is balanced with compressive residual stress of base metal [12].

2. Literature survey

Cottam et al. [11] studied the effect of both type of phase transformation on stress formation. They had reported that the martensitic transformation is more complex and help to reduce the magnitude of residual stress in transformed zone. During cooling process, transformation of austenite to martensite results in BCT structure formation that leads to increase in volume, as shown in Fig. 2 [13]. It has been reported that the precipitation process can reduce residual stress through load sharing. The effect of the martensite transformation is slightly more complex and acts to reduce the residual stress level in the transformed region. The inflection in the residual stress level just beyond the processing interface was attributed to point at which the martensitic transformation ceases resulting in an increase in the observed stress levels in the adjacent untransformed region. The increase the volume of transformed martensite reduces tensile residual stress levels and moves the location of the peak residual stress deeper into the substrate, which may be beneficial to the service life of a component.

A lot of work have been performed related to study of effect of welding process, groove geometry, welding parameters, and number of welding passes on shrinkage and shrinkage stress in pipe and plate weldments. Ghosh et al. [14] performed an analytical study on shrinkage stress mode, magnitude and distribution in different quadrants of GMAW and pulse GMAW welded pipe for different weld groove designs. The mode and magnitude of shrinkage stress in different quadrant was observed to be non-uniform and varied as a function of welding process, parameters and groove geometry. Pulse GMAW process has resulted in lower magnitude and uniform distribution of transverse shrinkage stress compared to GMAW. Higher the heat input during the welding process has resulted in higher magnitude of transverse shrinkage stress. For constant heat input, narrow groove design produced the lower shrinkage stress compared to conventional groove design. The multi-pass welding, the weld metal is subjected to localized solidification shrinkage [15]. The repetitive influence of thermal cycle from subsequent weld passes affects the development of stress in weld groove upto certain extent, and finally it causes a continuous change in groove design and groove area with every weld passes [16]. The change in groove size with subsequent pass results in groove angle variation and it will not be uniform at all location in each quadrant of pipe. The change in groove size and groove area was observed to be more in the case of V-groove weld design than narrow-groove [22] and this occurred due to less weld metal deposition in narrow groove. Ghosh et al. [17] studied the effect of Pulse GMAW and GMAW process on transverse shrinkage stress and distortion of thick butt welded plate.

It was observed that use of pulse GMAW produced low shrinkage stress, bending stress, and distortion compared to GMAW process. For given heat input, narrow groove weld design produced the lower stresses and distortion compared to V groove design but too much narrow groove was resulted in higher bending stress. For narrow groove weld design with pulse GMAW, about 35–45% reduction in transverse shrinkage was reported compared to conventional V groove pulse GMAW and SMAW [18]. Number of works have also reported related to 3D finite element (FE) simulation of residual stress and distortion. Yaghi et al. [19] performed a comparative study between numerically and experimentally evaluated residual stress value for P91 pipe weldments and showed a good agreements between the results. The residual stresses at outer surface was measured using X-ray diffraction while inner surface residual stress measurement performed using deep-hole drilling technique. Paddea et al. [7] performed an experimental study to measure the residual stress distribution in P91 girth pipe weldment and also study the effect of PWHT on their magnitude and distribution. The boundary of HAZ and base metal (IC-HAZ) showed the maximum tensile residual stress value about 600 MPa. The maximum tensile hydrostatic stress (400 MPa) was also observed near the vicinity of HAZ. The PWHT was resulted in considerable lowering in residual tensile stress (about 24% of yield strength of base metal) and hydrostatic stress (50 MPa). The compressive residual stress was reported in weld fusion zone near the final weld pass. Venkata et al. [20] studied the effect of PWHT on residual stress distribution in electron beam welded P91 plate. Kim et al. [21] predicted the residual stress distribution in P91 welded structure by using the neutron diffraction technique and to enhance the quality of results, the experimental results fairly matched with the numerical results obtained from FE simulation. Welding sequence have observed a great influence on residual deformation. Sattari-Far and Javadi [22] studied the welding sequence effect on distortion in pipe-pipe butt joints. The experimental results were validated with numerically obtained value. Welding leads the diametrical variation in pipe that mainly depend on the welding sequence. The diametrical variation in welding section was observed to be decreased (negative) and became zero at some distance away from the welding section and afterwards increased. Deng et al. [15] performed the residual stress estimation in multi-pass butt-welded thick pipe by strain gauge method and the experimentally observed residual stress value matched with numerically obtained residual stress value from 2-D axi-symmetric FE model. Procter and Beaney [23] had studied the residual stress measurement using the hole drilling method. At the initial stage of the work, the stress measurement was performed using the mechanical method and reported that no addition stresses are inducing during the drilling process. The plastic yielding was reported at the edge of hole in yield stress range of 0.25–0.5. The plasticity results in the error as the level of applied stresses increased above 60 percent of the yield strength of the material. In steel specimen, the plasticity error estimation was reported about 10–30 percent when induced residual stresses lead to the 70 percent of yield strength of work material [24]. Zhou and Rao had worked on the error analysis in the residual stress measurement by hole drilling technique [25]. It was concluded that error can be accepted when one of the strain gauge is used as a dummy point. Lin and Chou [26] reported the plasticity error in hole drilling process for the SS 304 austenitic steel, low carbon steel and Al 5052 aluminum alloy. It was reported that error can be neglected in case of the residual stress less than 65 percent of yield stress while the error was in the range of 32–47 percent at the 95 percent of yield stress of the material. For the plane stress biaxial state of stress, the plasticity error in residual stress measurement was reported by the Gibmeier et al. [27]. It was reported that the local plastic deformation during the hole drilling led to the high relief of strain that results in over estimation of the residual stresses. Vangi and Tellini had studied the effect of the parameters such as loading, geometrical and material on the measurement of residual stresses by the hole drilling technique [28]. In welded sample, the plasticity error in residual stress measurement was studied by the Moharami and Sattari-Far [29]. They studied the plasticity error by performing the uniaxial tensile experiments with pre existing hole and extended the work in their numerical modeling for biaxial stress state for the different material and loading combinations.

A detailed study on the effect of weld groove geometry on transverse shrinkage stress and residual stress of P91 pipe welds have not been observed in the literature review. The plasticity error estimation in blind hole drilling technique has also not been reported for the P91 steel.

From literature it has been noticed that the milling tool is generally used for the measurement of residual stresses in blind hole drilling which is generally affected by the wear and tear. In present work, effort has been made to study the effect of plasticity and stress concentration error on residual stress measurement by blind hole drilling technique. The strain gauge rosette of diameter 2.0 mm was used. Initially the calibration of the rosettes were performed using the uniaxial loading. For biaxial loading, 3-D finite element (FE) method was applied. Correlations were developed based on the output of finite element and regression model which was further utilized in residual stress calculation in P91 welded pipe.

3. Experimental details

3.1. *Groove design and welding process parameters*

Experimental setup for pipe welding, groove design for pipes, grooved P91 pipe, welded P91 pipe and welding process parameters are discussed in previous work [30]. The as-received P91 pipe was used for the experimental work. The P91 pipe was received in normalized and tempered condition. The normalizing is performed to develop untempered lath martensitic microstructure with negligible precipitates [31] however, some fine Nb-rich MX precipitates remain in the microstructure [32]. The tempering was performed to overcome the brittleness and evolution of new V and Nb-rich MX and Fe, Mo and Cr-rich $M_{23}C_6$ precipitates [33]. The schematic of the microstructure evolution in normalizing and after the tempering is shown in Fig. 3 [34,35]. In the present investigation, for the purpose of GTAW of P91 steel, AWSER90S-B9 (9CrMoV-N) filler wire was selected. The chemical compositions of the filler wire and base metal are given in Table 1. For

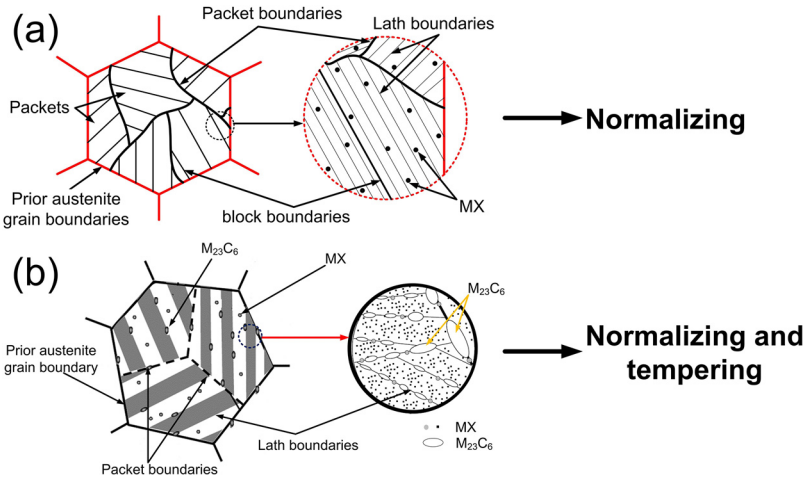

Fig. 3 – Schematic of microstructure evolution in normalized and tempered condition of P91 steel.

Table 1 – Chemical composition of base metal and filler wire (wt.%).

Element	Chemical composition (%)													
	C	Mn	P	S	Si	Cr	Mo	V	N	Ni	Cu	Nb	Ti	Fe
Base metal	0.12	0.54	<0.02	0.01	0.27	8.48	0.95	0.24	<0.02	0.35	0.05	0.05	0.01	Bal.
Filler metal	0.12	0.50	<0.002	–	0.30	9.0	0.90	0.20	0.02	0.50	–	0.05	<0.002	Bal.

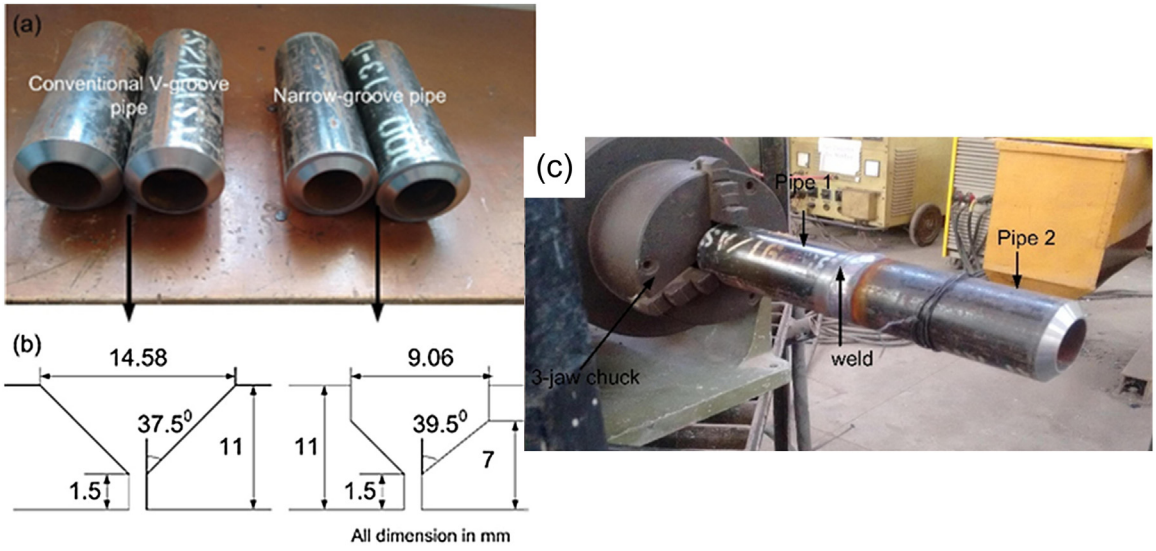

Fig. 4 – (a) Grooved pipe, (b) V-groove and narrow groove design, (c) welding set-up with welded pipe.

experimental work, P91 pipe having 11 mm thickness and 60.3 mm outer diameter was selected. The welding set-up, grooved pipe and pipe after welding are shown in Fig. 4. The schematic of weld passes arrangement for V-groove and narrow-groove pipe welds are shown in Fig. 5(a) and (b), respectively. The welding process parameters are depicted in Table 2. To maintain the linear travel speed of 2.11 mm/s during the filling pass, a stepper-motor controlled fixture was used. The preheat temperature of 150 °C and interpass temperature in the range of 150–250 °C were selected. For the shielding purpose, pure argon gas was used with a flow rate of 15 l/min.

3.2. *Plasticity error and measurement of residual stresses in welded pipe*

To measure the residual stress in pipe weldments, blind hole drilling technique was utilized using strain gauge rosette. Plasticity effect was also considered during the hole drilling process that might be lead to local yielding of the drilled hole boundary. To study the plasticity error estimation, P91 plates are selected. The as-received material properties are given in Table 3. To study the error estimation for residual stress measurement, the hole diameter of 2 mm was selected. The strain rosette, drilled hole diameter and depth are shown in Table 4.

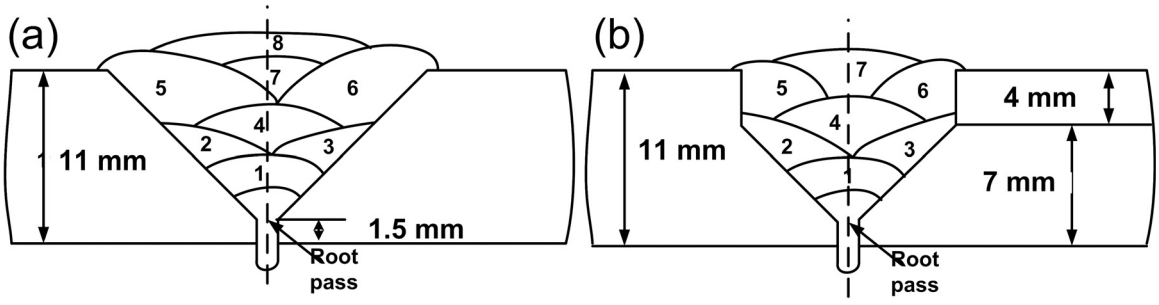

Fig. 5 – Schematic of weld passes: (a) V-groove, (b) narrow-groove.

Table 2 – Welding process parameter [36].

No. of passes	Welding current (amp)	Arc voltage (V)	Travel speed (mm/s)	Welding current (amp)	Arc voltage (V)	Travel speed (mm/s)
	Conventional V-groove			Narrow-groove		
Rot pass	105–115	12	1.47	105–115	12	1.47
1	110–115	12–14	2.11	110–115	12–15	2.11
2	120–125	12–15	2.11	110–115	12–15	2.11
3	118–124	14–16	2.11	112–120	14–16	2.11
4	120–123	12–14	2.11	118–124	15–18	2.11
5	110–115	18–20	2.11	118–124	14–18	2.11
6	112–120	14–16	2.11	115–120	14–15	2.11
7	120–125	12–14	2.11	114–118	13–16	2.11
8	120–125	12–15	2.11	–	–	–

Table 3 – Mechanical properties of P91 steel plate in as-received state.

P91 steel	Yield strength (MPa)	Tensile strength (MPa)	Elongation (%)	Hardness (HV)	Toughness (J)
	475	715	21	248	200

Table 4 – Rosette type, drilled hole diameter and depth.

Material	Strain rosette	Drilled hole diameter (mm)	Drilled hole depth (mm)
P91 steel	FRS-2-11	2.0	2.0

To estimate the calibration coefficient, a standard methodology was opted and tensile specimens were prepared. A cobalt-based end milling cutter was utilized to make a hole at the center of strain rosette. The strain rosette was attached to tensile specimen having 2 mm drilled hole diameter as shown in Fig. 6(a). Along the direction of rosette element number 3, two single element strain gauges (4 and 5) were attached. Initially, load was applied in various steps up to the 90% of yield strength of P91 steel, before drilling the hole. The strains were recorded in each load steps by keeping the strain gauge element 3 in loading direction. After that a blind hole of 2 mm diameter were made at the center of strain rosette. After the blind hole drilling, tensile load was applied again as per initial process and strains were recorded. The tensile specimen used for plasticity test is shown in Fig. 6(b).

To measure the residual stress in P91 welded pipe, blind hole drilling technique was utilized as per *ASTM E837-13a* [37,38]. The strain rosette is attached at the surface and make a hole at the center of strain rosette to relieve the strains. The drilling process is attributed to the stress relaxation around the hole due to the material removal. The released strains are used to calculate the residual stress. A hole of depth 2 mm and diameter of 2 mm was drilled at the center of the strain rosette by the end mill cutter and record the relaxed strain using the data logger. In P91 welded pipe, residual stresses were measured at the center of the weld and in HAZ. The set up for hole drilling is shown in Fig. 7. The induced plasticity error has been taken in to consideration in the evaluation of residual stress. The post weld heat treatment (PWHT) effect on mechanical properties have been reported in many of the research work but the study of PWHT on effect of residual stress have been observed in very few works [7,34,39,40]. According to the ASME Boiler and Pressure Vessel Code SA-335 [41], PWHT for P91 weldments recommended in temperature range of temperature of 730–770 °C for 1 h, but American Welding Society (AWS) suggests that PWHT should be carried out at 730–760 °C for 1 h [42]. To achieve the appropriate weld toughness, a Larson–Miller parameter '*P*' ≥ 21 is desirable for the heat treatment [7]. The Larson–Miller parameter *P* is given by;

$$P = K(\log t + C)\times 10^{-3}$$

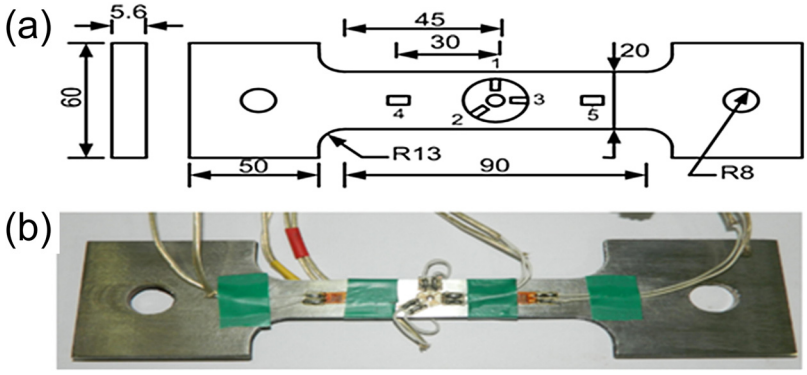

Fig. 6 – Tensile specimen: (a) schematic (1, 2 & 3: strain rosette elements, 4 & 5: single element strain gauge) & (b) actual (all dimensions in mm).

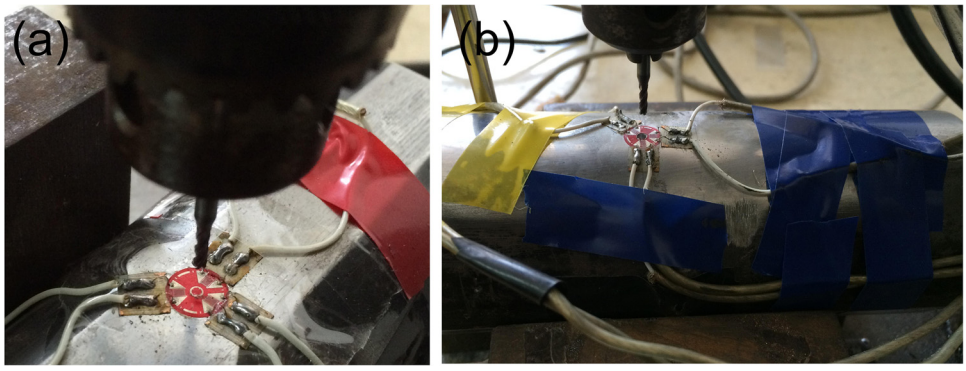

Fig. 7 – Residual stress measurement set up: (a) before drilling & (b) after drilling.

where 'k' is the soak temperature in Kelvin, 't' is the holding time in hours, and 'C' is the material specific constant. For the value of C = 21, the PWHT temperature is calculated about 755 °C for 2–3 h. For industrial purpose, both AWS and ASME recommended the post weld duration about 1 h. In present work PWHT was performed at 760 °C for 2 h and study their effect on the residual stresses as per reference [43].

4. Results and discussion

4.1. *Plasticity error estimation in uniaxial loading*

The magnitude and orientation of principle residual stress can be estimated using Eqs. (1)–(3), as shown below [38]. The maximum principle stress (σ_{max}) and minimum principle stress (σ_{min}) were calculates using Eqs. (1) and (2), respectively;

$$\sigma_{max} = \frac{\epsilon_1 + \epsilon_3}{4\overline{A}} + \frac{1}{4\overline{B}}\sqrt{(\epsilon_3 - \epsilon_1)^2 + (\epsilon_3 + \epsilon_1 - 2\epsilon_2)^2} \quad (1)$$

$$\sigma_{min} = \frac{\epsilon_1 + \epsilon_3}{4\overline{A}} + \frac{1}{4\overline{B}}\sqrt{(\epsilon_3 - \epsilon_1)^2 + (\epsilon_3 + \epsilon_1 - 2\epsilon_2)^2} \quad (2)$$

$$\tan 2\alpha = \frac{\epsilon_3 + \epsilon_1 - 2\epsilon_2}{\epsilon_3 - \epsilon_1} \quad (3)$$

where ε_1, ε_2 and ε_3 are the strains readings of strain rosette elements 1, 2 and 3, respectively. The angle between element 1 and minimum principle stress are presented by α. The schematic of three element strain gauge rosette is shown in Fig. 8.

In Eqs. (1) and (2), calibration coefficient $\overline{A}$ and $\overline{B}$ stated are calculated using Eqs. (4) and (5) [38]. The difference of strain reading was calculated from tensile testing with and without the hole in the strain rosette. The stress is applied in fraction of the yield strength of the material. The difference of the strain reading in principle direction of 1 and 3 before and after drill is termed as $\varepsilon_{1\,cal}$ and $\varepsilon_{3\,cal}$. The variations of coefficients $\overline{A}$ and $\overline{B}$ with respect to the ratio of applied stress to yield strength of work materials is depicted in Fig. 9(a). Eqs. (6) and (7) are used to calculate the calibration coefficients *a* and *b* used in residual stress measurement [38]. The average values of $\overline{A}$ and $\overline{B}$ are presented in Table 5.

$$\overline{A} = \frac{\epsilon_{3\,cal} + \epsilon_{1\,cal}}{2\sigma_{app}} \quad (4)$$

$$\overline{B} = \frac{\epsilon_{3\,cal} - \epsilon_{1\,cal}}{2\sigma_{app}} \quad (5)$$

$$\overline{A} = -\frac{(1+\mu)a}{2E} \quad (6)$$

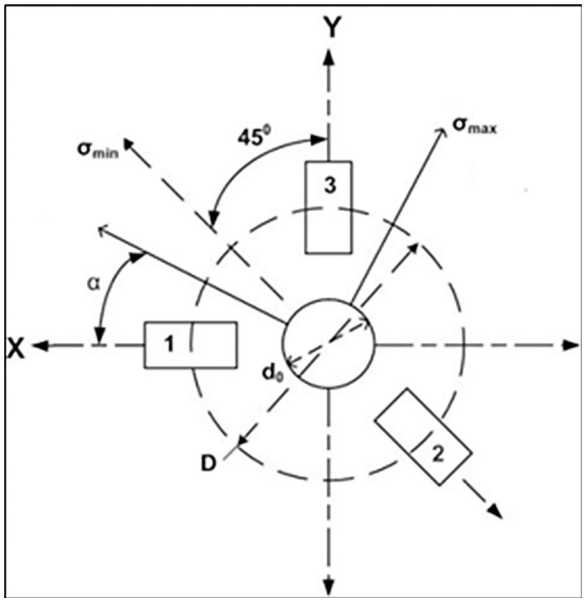

Fig. 8 – Schematic of three element strain gauge rosette.

$$\overline{B} = -\frac{b}{2E} \tag{7}$$

To calculate the applied stress as per *ASTM E837-13a* [37,38], strains reading (ε_1, ε_2 & ε_3) obtained from strain rosette were utilized while the single element strain gauge is used to calculate the applied stress away from the hole but within gauge length.

Eq. (8) is used to estimate the error in uniaxial loading direction.

$$\text{Error } (\%) = \frac{(\sigma_{ASTM} - \sigma_{app})}{\sigma_{app}} * 100 \tag{8}$$

where σ_{ASTM} is the stress calculated from (ASTM E837-13a) as per the strain readings of strain rosette.

The error variation with respect to ratio of applied stress and yield strength of work materials (σ_{app}/σ_y) is presented in Fig. 9(b). The induced error was observed to be increased with increase in the ratio of applied stress to yield strength of material. Hence it can be stated that in uniaxial loading, the error value increases with higher applied stress. The error was measured in range of 3–44 percent.

4.2. *Error estimation for biaxial stress analysis*

The % error value was observed to be increased with increase in applied stress. The value obtained for uniaxial loading might not be used for the multiiaxial loading. In P91 steel, higher yield strength of material might be lead to high residual stress. It is difficult to estimate the exact value of plastic yielding magnitude around the blind hole. A 3-D numerical modeling was performed to estimate the biaxial state of stress. Fig. 10 shows the model and meshing for the blind hole. Ansys program was used to make the 3-D model and after that meshing was performed by selecting the 8 node SOLID 185 element in ANSYS for structural stress analysis. A 3-D FE model with dimensions 20 mm × 20 mm × 5.6 mm were prepared for the 2 mm blind hole geometry. For 2 mm blind hole geometry, elements and nodes were 67012 and 35024, respectively.

Initially 2 mm hole was made and applied the uniaxial loading as per experiments. As per experiments, for numerical model the applied load value was increased gradually in along the sample axis. The response of the nodes that falls under the area of strain rosette elements have been measured and estimate the average strain value. The estimated average strain value obtained from the experiments was compared with the uniaxial experimentally strain value. The strain value obtained from the uniaxial tensile tests and from the Finite element modeling showed a good agreement as given in Table 6. In biaxial stress analysis, stresses were applied in both directions and four stress ratio (SR), transverse to longitudinal stress ($\sigma_{Tapp}/\sigma_{Lapp}$ = 0.2, 0.6, 0.8 & 1) were used. For each stress ratio, applied longitudinal stress (σ_{Lapp}) was varied from 0.5σ_y to σ_y. To estimate the correlations for calculation of residual stress error estimations, the strain data obtained from the numerical analysis was utilized. The correlation was developed for strain gauge rosette having 2 mm hole diameters for P91 steel.

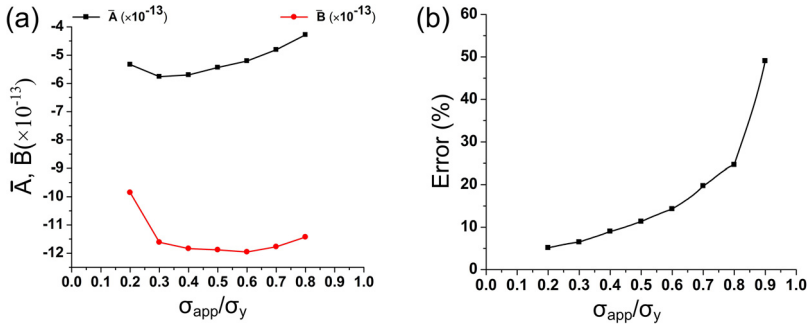

Fig. 9 – (a) Variation of calibration coefficient $\overline{A}$ and B, (b) percentage error vs. applied stress ratio.

Table 5 – Calibration Coefficients.

Material	$\overline{A}$ (×10^{-13})	$\overline{B}$ (×10^{-13})	*a*	*b*
P91 steel	−4.58	−11.12	0.17	0.48

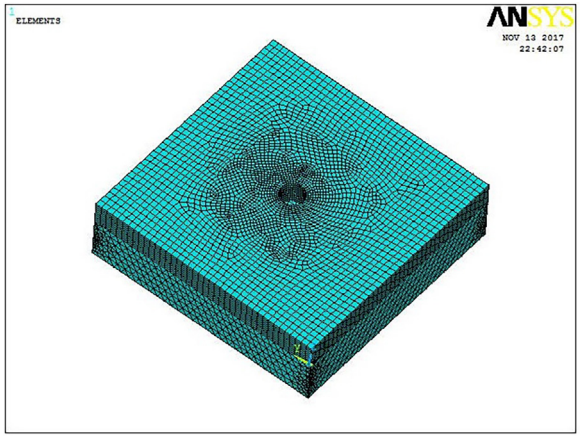

Fig. 10 – Meshed model for estimation of error in uniaxial and biaxial loading.

Table 6 – Comparison of strain values (in microns).

Material	Experimental		Predicted	
	ε_1	ε_3	ε_1	ε_3
P91 steel (2 mm hole dia.)	−267	745	−247	720

In blind hole drilling method, three element strain rosette used for the strain calculation is shown in Fig. 11. The strains value (ε_1, ε_2 & ε_3) were calculated form the FE model by taking the average of strain value at each nodes under the area of gauge elements. The strains value were utilized to calculate the longitudinal and transverse stress (σ_{Lastm} & σ_{Tastm}) based on ASTM E837-13 [37]. The percentage error of stresses in longitudinal and transverse directions are calculated using Eqs. (9) and (10), respectively.

$$\text{Error } (\%) = \frac{(\sigma_{Lastm} - \sigma_{Lapp})}{\sigma_{Lapp}} * 100 \quad (9)$$

$$\text{Error } (\%) = \frac{(\sigma_{Tastm} - \sigma_{Tapp})}{\sigma_{Tapp}} * 100 \quad (10)$$

Fig. 11 shows the percentage errors for longitudinal and transverse directions. The transverse error observed for stress ration of 0.2 was much higher than other errors value calculated for other stress ratio. It was observed that for applied biaxial stress close to the yield strength of material, longitudinal and transverse errors were lowest, as shown in Fig. 11. Fig. 11 shows the measurement in the error in axial and transverse direction for biaxial loading. The load is applied in fraction of the yield strength of the material. As the applied load approaches to the yield strength of the material, the error in longitudinal direction tends to decrease while in transverse direction tends to increase or almost remain constant. Further, if the load applied in both the direction will be same then error will also be high in both axial and transverse direction. When load applied in transverse direction decreases as compared to axial direction, the error will also decrees both in axial and transverse direction. In order to make the relationship between the corrected stress value and ASTM calculated residual stresses value, regression analysis was performed using the MINITAB software. Analysis of variance (ANOVA) was used to build the relations between the control factor and responses. Table 7 depicts the result of ANOVA. The coefficient of determination R^2, the proportion of variability in the data sample is 98.5 % as indicated in Table 7. The adjusted R^2 is a measure of proportion of variation in the dependent variable. Table 7 also indicate sequential sum of square (Seq SS), adjusted sum of square (Adj SS) and adjusted mean square (Adj MS). The adjusted sum of squares, calculated by MINITAB, are determined by the addition of each particular term to a regression model considering the effect of other terms also in the model. The ANOVA is useful to investigate the significance of factors and their interaction on the responses. The ratio of the ASTM calculated stresses to yield strength (σ_{Tastm}/σ_y and σ_{Lastm}/σ_y) were also utilized to develop the relationship between ASTM calculated and corrected residual stress value. Eqs. (11) and (12) shows the relations. Analysis of variance for P91 steel of 2 mm hole diameter is shown in Table 7. The error

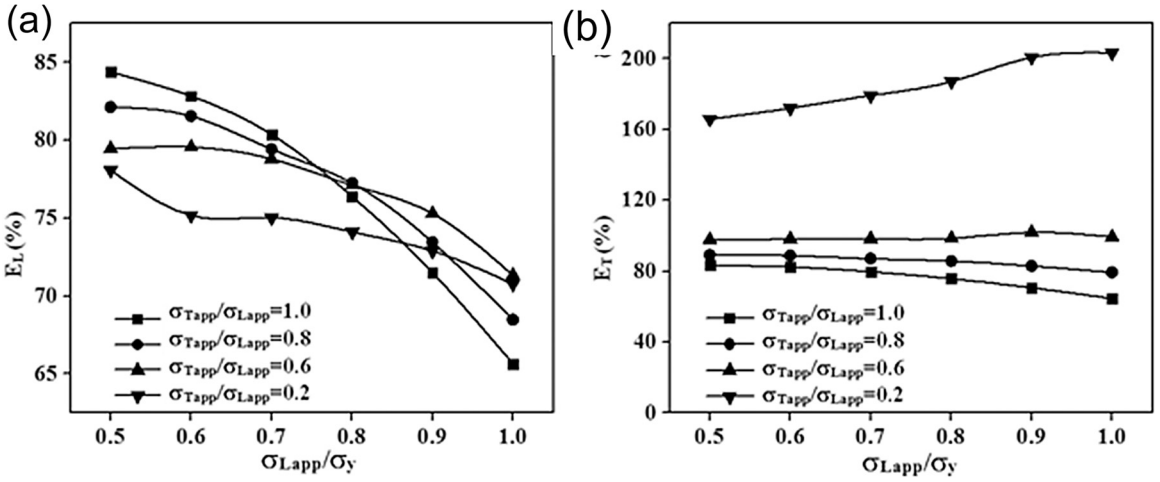

Fig. 11 – Percentage error; (a) longitudinal & (b) transverse for 2 mm hole.

Table 7 – ANOVA Table of σ_L and σ_T for P91 steel (2 mm hole).

Analysis of variance for σ_L (response surface regr: R-Sq = 98.5%, R-Sq(adj) = 98.4%)

Source	DF	Seq SS	Adj SS	Adj MS	F	P
Regression		3	125 750	125 750	41 916.8	1219.14
Linear	3	125 750	125 750	41 916.8	1219.14	0
Residual error	20	687	687	34.4		
Total	23	126 437				

Analysis of variance for σ_T (response surface regr: R-Sq = 99.4%, R-Sq(adj) = 99.3%)

Source	DF	Seq SS	Adj SS	Adj MS	F	P
Regression	3	276 248	276 248	92 082.7	1152.27	0
Linear	3	276 248	276 248	92 082.7	1152.27	0
Residual error	20	1598	1598	79.9		
Total	23	277 846				

Table 8 – Results of residual stresses.

Welding condition	Groove design	Center of the weld				Center of HAZ			
		ASTM value of residual stress		Corrected Residual stress		ASTM value of residual stress		Corrected Residual stress	
		σ_T	σ_l	σ_T	σ_l	σ_T	σ_l	σ_T	σ_l
As-welded	V-Groove	226 ± 15	220 ± 12	114 ± 10	112 ± 8	104.69	137.98	28.54	71.79
	Narrow-groove	108 ± 5	148 ± 17	45 ± 2	65 ± 11	92.93	100.02	27.09	42.94
PWHT	V-Groove	105	85	52	23	49	54	19	4
	Narrow-groove	57	73	23	15	51	54	20	3

in residual stress calculation depends on so many factors like biaxial stress ration, yield strength of material, and applied stress.

$$\sigma_L = -32.7 - 241\sigma_{Lastm}/\sigma_y - 0.006\sigma_{Tastm} + 1.2\sigma_{Lastm} \quad (11)$$

$$\sigma_T = -6.21 + 404.58\sigma_{Tastm}/\sigma_y - 0.26\sigma_{Tastm} + 0.109\sigma_{Lastm} \quad (12)$$

4.3. *Residual stresses*

Axial and hoop stress results are depicted in Table 8. At the center of weld fusion zone, predicted nature of axial and hoop stress was in tensile manner. The maximum predicted hoop stress in weld zone was about 226 ± 15 MPa in V-groove weld design while minimum was about 108 ± 5 MPa in narrow groove design. The maximum and minimum predicted axial stress were 220 ± 12 MPa and 148 ± 17 MPa for V-groove and narrow-groove design, respectively. At the center of heat affected zone (HAZ) (approximately 8 mm for V-groove and 7 mm for narrow groove design), the magnitude of residual stresses were observed to be in tensile nature with lower magnitude as compared to weld fusion zone. In V-groove design, magnitude of axial and hoop stresses were 137.98 MPa and 104.69 MPa, respectively while in narrow groove design, magnitude were 100 and 92.93 MPa, respectively.

4.4. *Effect of PWHT on residual stresses*

After the post weld heat treatment of 760 °C for 2 h, a considerable lowering in magnitude of residual stress were observed while nature remains same, as given in Table 6. At the weld center, the maximum hoop and axial stresses were measured to be 105 MPa and 85 MPa, for V-groove design. For narrow groove design, hoop and axial stresses were measured to be 57 MPa and 73 MPa, respectively, which was approximately half of the previous value (as-welded condition). In HAZ, axial stress was observed only 0.66% of the yield strength of the material. During the welding process, less volume of weld metal was deposited in narrow-groove weld as compared to V-groove weld and it might be cause of lower magnitude of residual stresses in the narrow groove weld design as compared to V- groove weld design. Lower volume of deposited metal leads to less resistance to shrinkage and lower residual stresses in narrow groove weld.

4.5. *Corrected residual stresses*

The corrected residual stresses values were calculated using Eqs. (11) and (12). The yield strength of material was considered to be 450 MPa. The maximum corrected axial residual stress value (112 ± 8 MPa) was obtained for V-groove design which was 30.66% of the yield strength of the material.

The corrected residual stresses value obtained for the V-groove and narrow-groove design were too much low as compared to yield strength of the material. The corrected hoop stress value was measured to be 114 ± 10 MPa for V-groove design. For narrow groove design corrected axial and hoop stress value were measured to be 65 ± 11 and 45 ± 2 MPa, respectively which was much less than the yield strength of P91 steel. After the PWHT, a drastic decrease in corrected residual stress was measured, as given in Table 6. For narrow-groove design, minimum corrected axial stress was measured to be 3 MPa.

4.6. *Comparison of residual stresses and shrinkage stress*

In previous study, Pandey et al. [30] had studied the effect of groove design on the transverse shrinkage stresses in P91 welded pipe for similar welding conditions and process parameters. Pandey et al. [30] have observed the average transverse shrinkage stresses of 164.33 and 110.33 MPa, for V-groove and narrow-groove design, respectively. The transverse shrinkage stress was approximately 34% of the yield strength of material for V-groove and 23% of the yield strength of material for narrow groove weld design.

From current and previous study, a comparison was performed in estimated residual stress and transverse shrinkage stresses for P91 welded pipe of 11 mm thickness. In previous study, the transverse shrinkage stresses were measured to be 164.33 and 110.33 MPa, for V-groove and narrow-groove design, respectively. For V-groove design, the axial and hoop stresses were measured 112 ± 8 MPa and 114 ± 10 MPa, which was less than the transverse shrinkage stresses developed in V-groove weld design. For narrow-groove design, the axial and hoop stresses were measured 65 ± 11 MPa and 45 ± 2 MPa. The axial and hoop stresses measured for the narrow-groove design were observed to be much less than the transverse shrinkage stresses (110.33 MPa). The comparison of axial stress, hoop stress, and transverse shrinkage stress are shown in Fig. 12.

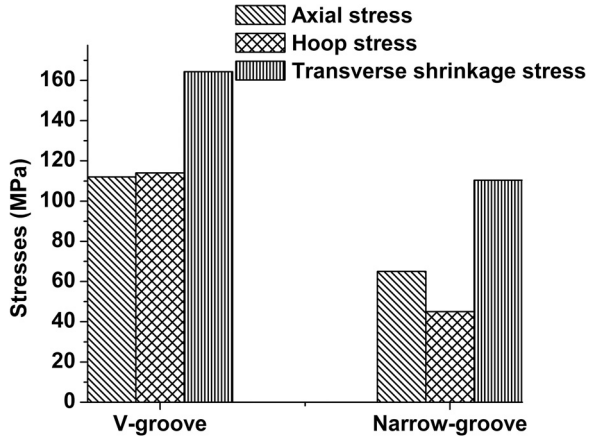

Fig. 12 – Comparison of residual stresses and transverse shrinkage stress for V-groove and narrow-groove design.

5. Conclusions

In present investigation, the nature of plasticity error has been observed for both uniaxial and biaxial loading for blind hole drilling method. A numerical relation has been developed to estimate the corrected transverse and axial stress in P91 steel which was successfully implemented in corrected residual stress calculation in P91 welded pipe of 11 mm thickness. The nature of axial and hoop stresses in weld fusion zone and heat affected zone of P91 welded pipe was observed to be tensile. The ASTM calculated axial and hoop stresses for V-groove design were 220 ± 12 and 226 ± 15 MPa, respectively. The magnitude of axial and hoop stresses were observed to be less for narrow-groove design. The corrected residual stresses value were measured to be much lower than the ASTM estimated residual stresses value. In HAZ, corrected axial stresses were measured to be 71.79 MPa and 42.94 MPa for V-groove and narrow-groove design. After the PWHT, the axial stress were measured to be 4 MPa and 3 MPa for V-groove and narrow-groove design. Axial and hoop stresses measured for narrow-groove was lower than the V-groove design.

Ethical statement

I ensure that the work described has been carried out in accordance with Publishing Ethics.

Appendix A. Supplementary data

Supplementary data associated with this article can be found, in the online version, at doi:10.1016/j.acme.2018.02.007.

REFERENCES

[1] J. Hald, Microstructure and long-term creep properties of 9–12% Cr steels, Int. J. Pressure Vessels Piping 85 (2008) 30–37. http://dx.doi.org/10.1016/j.ijpvp.2007.06.010.

[2] C. Pandey, M.M. Mahapatra, Evolution of phases during tempering of P91 steel at 760 °C for varying tempering time and their effect on microstructure and mechanical properties, Proc. Inst. Mech. Eng. Part E: J. Process Mech. Eng. 231 (2017), http://dx.doi.org/10.1177/0954408916656678.

[3] C. Pandey, N. Saini, M.M. Mahapatra, P. Kumar, Hydrogen induced cold cracking of creep resistant ferritic P91 steel for different diffusible hydrogen levels in deposited metal, Int. J. Hydrogen Energy 41 (2016) 17695–17712. http://dx.doi.org/10.1016/j.ijhydene.2016.07.202.

[4] C. Pandey, A. Giri, M.M. Mahapatra, P. Kumar, Characterization of microstructure of HAZs in as-welded and service condition of P91 pipe weldments, Met. Mater. Int. 23 (2017) 148–162., http://dx.doi.org/10.1007/s12540-017-6394-5.

[5] S.H. Babu, G. Amarendra, R. Rajaraman, C.S. Sundar, Microstructural characterization of ferritic/martensitic steels by positron annihilation spectroscopy, J. Phys.: Conf. Ser. (ICPA-16) 443 (2013) 1–6. http://dx.doi.org/10.1088/1742-6596/443/1/012010.

[6] B. Silwal, L. Li, A. Deceuster, B. Griffiths, Effect of postweld heat treatment on the toughness of heat-affected zone for Grade 91 steel, Weld. Res. 92 (2013) 80s–87s.
[7] S. Paddea, J.A. Francis, A.M. Paradowska, P.J. Bouchard, I.A. Shibli, Residual stress distributions in a P91 steel-pipe girth weld before and after post weld heat treatment, Mater. Sci. Eng. A 534 (2012) 663–672. http://dx.doi.org/10.1016/j.msea.2011.12.024.
[8] C. Pandey, M.M. Mahapatra, P. Kumar, N. Saini, Diffusible hydrogen level in deposited metal and their effect on tensile properties and flexural strength of P91 steel, J. Eng. Mater. Technol. 139 (2017) 1–11. http://dx.doi.org/10.1115/1.4035764.
[9] C. Pandey, A. Giri, M.M. Mahapatra, On the prediction of effect of direction of welding on bead geometry and residual deformation of double-sided fillet welds, Int. J. Steel Struct. 16 (2016) 333–345. http://dx.doi.org/10.1007/s13296-016-6007-z.
[10] C. Pandey, M.M. Mahapatra, P. Kumar, N. Saini, Some studies on P91 steel and their weldments, J. Alloys Compd. 743 (2018) 332–364.
[11] R. Cottam, V. Luzin, K. Thorogood, Y.C. Wong, M. Brandt, The role of metallurgical solid state phase transformations on the formation of residual stress in laser cladding and heating, Mater. Sci. Forum 777 (2014) 19–24. http://dx.doi.org/10.4028/www.scientific.net/MSF.777.19.
[12] A. De, T. Debroy, A perspective on residual stresses in welding, Sci. Technol. Weld. Join. 16 (2017) 204–208. http://dx.doi.org/10.1179/136217111X12978476537783.
[13] A.H. Yaghi, T.H. Hyde, A.A. Becker, W. Sun, Finite element simulation of welding and residual stresses in a P91 steel pipe incorporating solid-state phase transformation and post-weld heat treatment, IMechE: J. Strain Anal. 43 (2008) 275–293. http://dx.doi.org/10.1243/03093247JSA372.
[14] P.K. Ghosh, R.R. Kumar, K. Devakumaran, Effect of pulse current on shrinkage stress and distortion in multi pass GMA welds of different groove sizes, Indian Weld. J. 43-s (2010) 14–23.
[15] D. Deng, H. Murakawa, W. Liang, Numerical and experimental investigations on welding residual stress in multi-pass butt-welded austenitic stainless steel pipe, Comput. Mater. Sci. 42 (2008) 234–244. http://dx.doi.org/10.1016/j.commatsci.2007.07.009.
[16] P. Dong, Residual stress analyses of a multi-pass girth weld: 3-D special shell versus axisymmetric models, J. Pressure Vessel Technol. 123 (2001) 207–213. http://dx.doi.org/10.1115/1.1359527.
[17] P.K. Ghosh, R.R. Kumar, A.K. Pramanick, Effect of pulse current on shrinkage stress and distortion in multi pass GMA welds of different groove sizes, Ind. Weld. J. Weld. J. 43-s (2010) 14–24.
[18] R. Anant, P.K. Ghosh, Experimental investigation on transverse shrinkage stress and distortion of extra narrow and conventional gap dissimilar butt joint of austenitic stainless steel to low alloy steel, in: Proceedings of the International Conference on Mining, Material and Metallurgical Engineering, 2014, 1–5.
[19] A.H. Yaghi, T.H. Hyde, A.A. Becker, W. Sun, G. Hilson, S. Simandjuntak, P.E.J. Flewitt, D.J. Smith, A comparison between measured and modeled residual stresses in a circumferentially butt-welded P91 steel pipe, J. Pressure Vessel Technol. 132 (2010) 1–10. http://dx.doi.org/10.1115/1.4000347.
[20] K.A. Venkata, S. Kumar, H.C. Dey, D.J. Smith, P.J. Bouchard, Study on the effect of post weld heat treatment parameters on the relaxation of welding residual stresses in electron beam welded P91 steel plates, Proc. Eng. 86 (2014) 223–233. http://dx.doi.org/10.1016/j.proeng.2014.11.032.
[21] S. Kim, J. Kim, W. Lee, Numerical prediction and neutron diffraction measurement of the residual stresses for a modified 9Cr–1Mo steel weld, J. Mater. Process. Technol. 209 (2009) 3905–3913. http://dx.doi.org/10.1016/j.jmatprotec.2008.09.012.
[22] Y. Sattari-Far, I. Javadi, Influence of welding sequence on welding distortions in pipes, Int. J. Pressure Vessels Piping 85 (2008) 265–274. http://dx.doi.org/10.1016/j.ijpvp.2007.07.003.
[23] E. Procter, E.M. Beaney, Recent developments in center – hole technique for residual-stress measurement, Exp. Tech. 6 (1982) 10–15.
[24] W.E. Nickola, Practical subsurface residual stress evaluation by the hole-drilling method, in: Proceedings of the Fifth International Congress on Experimental Mechanics, 1986, 126–136.
[25] H. Zhou, M.D. Rao, On the error analysis of residual stress measurements by the hole drilling method, J. Strain Anal. 28 (1993) 273–276.
[26] Y.C. Lin, C.P. Chou, Error induced by local yielding around hole in hole drilling method for measuring residual stress of materials, Mater. Sci Technol. 11 (1995) 600–604.
[27] J. Gibmeier, J.P. Nobre, B. Scholtes, Residual stress determination by the hole drilling method in the case of highly stressed surface layers, Mater. Sci. Res. Int. 10 (2004) 21–25.
[28] D. Vangi, S. Tellini, Hole-drilling strain-gauge method: residual stress measurement with plasticity effects, J. Eng. Mater. Technol. 132 (2010) 1–7. http://dx.doi.org/10.1115/1.3184030.
[29] R. Moharami, I. Sattari-Far, Experimental and numerical study of measuring high welding residual stresses by using the blind-hole-drilling technique, J. Strain Anal Eng. Design 43 (2008) 141–148. http://dx.doi.org/10.1243/03093247JSA378.
[30] C. Pandey, H.K. Narang, N. Saini, M.M. Mahapatra, P. Kumar, Microstructure and transverse shrinkage stress analysis in GTA welds of P91 steel pipe, Int. J. Steel Struct. 17 (2017) 763–774. http://dx.doi.org/10.1007/s13296-017-6030-8.
[31] C. Pandey, M.M. Mahapatra, P. Kumar, N. Saini, Homogenization of P91 weldments using varying normalizing and tempering treatment, Mater. Sci. Eng. A (2017), http://dx.doi.org/10.1016/j.msea.2017.10.086.
[32] K. Maruyama, K. Sawada, J. Koike, Strengthening mechanisms of creep resistant tempered martensitic steel, ISIJ Int. 41 (2001) 641–653. http://dx.doi.org/10.2355/isijinternational.41.641.
[33] C. Pandey, M. Mahapatra, Evolution of phases during tempering of P91 steel at 760 for varying tempering time and their effect on microstructure and mechanical properties, Proc. Inst. Mech. Eng. Part E: J. Process Mech. Eng. 664 (2016) 58–74. http://dx.doi.org/10.1177/0954408916656678.
[34] C. Pandey, M.M. Mahapatra, P. Kumar, N. Saini, Comparative study of autogenous tungsten inert gas welding and tungsten arc welding with filler wire for dissimilar P91 and P92 steel weld joint, Mater. Sci. Eng. A 712 (2018) 720–737. http://dx.doi.org/10.1016/j.msea.2017.12.039.
[35] N. Saini, C. Pandey, M.M. Mahapatra, R.S. Mulik, On study of effect of varying tempering temperature and notch geometry on fracture surface morphology of P911 (9Cr–1Mo–1W–V–Nb) steel, Eng. Fail. Anal. 85 (2018) 104–115. http://dx.doi.org/10.1016/j.engfailanal.2017.12.013.
[36] C. Pandey, M.M. Mahapatra, P. Kumar, N. Saini, Effect of normalization and tempering on microstructure and mechanical properties of V-groove and narrow-groove P91 pipe weldments, Mater. Sci. Eng. A 685 (2017) 39–49. http://dx.doi.org/10.1016/j.msea.2016.12.079.
[37] ASTM E837-13a, Standard Test Method for Determining Residual Stresses by the Hole Drilling Strain Gage Method, ASTM International, West Conshohocken, PA, 2013, http://dx.doi.org/10.1520/E0837-13A.2.
[38] TN-503, Measurement of Residual Stresses by the Hole Drilling Strain Gauage Method, Vishay Precision Group, 2010, pp. 19–33.

[39] C. Pandey, M.M. Mahapatara, P. Kumar, N. Saini, Dissimilar joining of CSEF steels using autogenous tungsten-inert gas welding and gas tungsten arc welding and their effect on δ-ferrite evolution and mechanical properties, J. Manufact. Process. 31 (2018) 247–259. http://dx.doi.org/10.1016/j.jmapro.2017.11.020.

[40] C. Pandey, M.M. Mahapatra, P. Kumar, N. Saini, J.G. Thakre, R. S. Vidyarthy, H.K. Narang, A brief study on δ-ferrite evolution in dissimilar P91 and P92 steel joint and their effect on mechanical properties, Arch. Civ. Mech. Eng. 18 (2018) 713–722. http://dx.doi.org/10.1016/j.acme.2017.12.002.

[41] D.J. Kotecki, Hydrogen reconsidered, Weld. J. 71 (1992) 35–43.

[42] American Welding Society, AWS D10.10/D10.10M-1999. Recommended Practices for Local Heating of Welds in Piping and Tubing, 1999.

[43] C. Pandey, M.M. Mahapatra, P. Kumar, N. Saini, Some studies on P91 steel and their weldments, J. Alloys Comp. (2018), http://dx.doi.org/10.1016/j.jallcom.2018.01.120.